

**OC3570 CRUISE REPORT ON  
TRANSMISSIVITY AND  
PHOTOSYNTHETICALLY ACTIVE  
RADIATION DATA ANALYSIS**

**Naval Postgraduate School  
Monterey, California**

**Ashley D. Evans**

**LCDR/USN**

**21 March 2002**

## **Introduction**

NPS students conducted a research cruise aboard the RV Point Sur from 1-4 February 2002. Although many types of oceanographic and atmospheric measurements were taken during the cruise, this report focuses on the results of a 24 hour time series containing optical transmissivity measurements, photo-synthetically active radiation measurements, and acoustic doppler current profiler measurements taken in Monterey Bay, figure (1), during leg two of the OC 3750 class cruise.

Monterey Bay has three major oceanic seasons: the upwelling season, fall oceanic season and the Davidson current season. The Davidson current season occurs during the late winter months from November to March and marks an annual minimum in primary phytoplankton productivity in Monterey Bay (Pennington et al., 1999). The cruise occurs near the end of the Davidson current season when biota productivity is low and sediment particulate is just beginning to increase from seasonal runoff.

Optical transmissivity is important for Naval research with the shift to littoral operations and the emergence of a brown water navy reliant on water clarity both for operational movement and weapons performance. A Wide array of naval operations requires knowledge of water clarity. These include, but are not limited to, Special Operations, Mine Warfare, Undersea Warfare, and Naval Intelligence.

This report aims to analyze the temporal water clarity features and variability of a small area in the upper portion of the Monterey Canyon. The analysis will point out significant features and coupling of water clarity changes to other coastal ocean processes that occur on the the same spatial and temporal scales.

## **2. Equipment**

### **A. Background**

Ambient light is often analyzed in a differential mode – sunlight intensity is measured both at the surface of the water and in the water column. This way, light availability and attenuation can be monitored. As sunlight enters the ocean, it begins to be absorbed and/or scattered. The upper portion of the ocean known as the euphotic zone extends from the surface down to the level where there is still adequate light to support photosynthesis in phytoplankton. There are varying technical definitions for the zone but nominally the euphotic zone is defined as the level where the entering energy is reduced to 1% of its original value (Widder, E., 1998). The actual depth level depends on the time of year, time of day, the clarity of the water and cloud cover.

Absorption and scattering are the two basic processes that alter light energy underwater. Absorption is a change of light energy into other forms of energy such as heat. Scattering involves a change in the direction of light energy propagation without any inherent loss of total energy content.

Textbooks define attenuation as the sum of absorption and scattering, figure (2). The energy lost from a well-collimated monochromatic beam in an attenuating medium given by equation 1:

$$I(z) = I(0)e^{-cz} \quad \mathbf{(1)}$$

where “c” is the beam attenuation coefficient made up of an absorption beam coefficient “a” and a scattering beam coefficient “b” where “(c = a + b)” and “z” is the distance the light is transmitted. The percent of light transmitted over a distance given by equation 2:

$$T(z) = \frac{I(z)}{I(0)} = e^{-cz} \quad \mathbf{(2)}$$

This simple relationship holds as long as the light is monochromatic. The transmissometer, (discussed later), is nearly monochromatic whereas the PAR sensor, (discussed later), deviates from the ideal case due to a wider spectrum response. This adjustment is handled by construction of a wavelength dependent beam attenuation coefficient and input in to the governing equation, (Biosperical Instruments, 1993)

The beam attenuation coefficient “c” can be divided into three parts: 1) Attenuation due to the water itself ( $c_w$ ); 2) attenuation due to suspended particulate matter ( $c_p$ ); and 3) attenuation due to dissolved materials (mostly humic acids or “yellow matter”) ( $c_y$ ). Each of these components has distinct spectral characteristics. Of special interest is the fact that yellow matter absorbs strongly in the blue part of the

spectrum and decreases exponentially with increasing wavelengths.

Yellow matter is a by-product of organic decay and found primarily in lakes, reservoirs and in near-shore waters. At 660 nm wavelength in the visible spectrum, the attenuation of yellow matter is negligible and most of the attenuation is due to particulate matter and seawater only.

### **B. Transmissometer**

To measure the transmissivity we used a 25 cm transmissometer manufactured by Sea Tech, Inc., figure (3). The instrument was mounted on the lower section of a Seabird CTD, figure (4), and took measurements at one meter intervals to within 10 meters of the bottom at canyon, wall and shelf stations.

Figure (5) shows a transmissometer outline drawing. The device measures in-situ beam transmission and the concentration of suspended matter in the water. Transmission is measured using a nearly monochromatic modulated Light Emitting Diode (LED) with a wavelength of 660 nm (red part of the spectrum), and a synchronous detector over a transmission distance of 25 cm. The instrument is not sensitive to ambient light, is temperature compensated, and is usable in depths up to 5000 meters, (Sea Tech Inc, 1998.).

### **C. Photosynthetically Active Radiation Detector**

Photosynthetically Active Radiation (PAR) is a term often associated with ambient light measurement. Sunlight consists of a wide spectrum of colors (wavelengths), but only a small band from 400-700 nm supports

ocean photosynthesis. The light energy intensity in this small band represents (PAR). A QSP-2001 Logarithmic Output Oceanographic Light Transducer PAR detector from Biospherical Instruments Inc. was mounted to the upper section of the Seabird CTD, figure (6), and took measurements at one meter intervals to within 10 meters of the bottom at canyon, wall and shelf stations and recorded PAR. Figure (7) shows a disconnected PAR detector. The white sphere on top is the radiation collector. The detector design allows the oceanographer to measure the widely varying light fields in the water column while taking measurements with the Seabird CTD. Its logarithmic output correlates well with the inherently depth dependent exponential decay of light in the ocean. The instruments spectral response is specifically designed to measure (PAR) between 400-700 nm with constant response and output in  $\mu\text{einsteins}/\text{cm}^2/\text{s}$ , a measure of photon irradiance in the water column, (Biospherical Instruments Inc, 1993.).

#### **D. Acoustic Doppler Current Profiler**

Acoustic Doppler Current Profilers (ADCP), figure (8), uses the well-known doppler effect principle to measure ocean currents by transmitting sound at a fixed frequency and listening to echoes returning from sound scatterers in the water where the doppler shift is governed by equation 3:

$$FD = 2 \times Fs \times (V/C) \times \cos(A) \quad (3)$$

The ship-borne ADCP uses multiple beams to obtain a velocity profile in three dimensions. The major assumption; entails assuming currents are homogeneous over layers of constant depth. The ADCP post processor breaks up the velocity profile into uniform segments called depth cells and calculates the three dimensional current (velocity) for each depth cell, (RD Instruments, 1996).

#### **E. Sea-viewing Wide Field of View Sensor**

Sea-viewing Wide Field Of View Sensor (SeaWiFS), figure (10), is a spectroradiometer mounted on the Sea Star polar orbiting satellite, figure (9). It operates on six channels covering both the visible and near infrared light wavelengths. In the ocean, light reflects off particulate matter suspended in the water, and undergoes absorption and emission primarily due to photosynthetic pigment (chlorophyll) present in the phytoplankton that respond to the visible light spectrum in the 400 – 700 nm wavelengths. The net result of these optical interactions is light radiating from the ocean surface – the measurable water leaving radiance. Radiometers measure the radiance intensity at given wavelengths. The radiances in the given bands (green, blue, red); (520 nm, 443 nm, 660 nm) are post processed through algorithms to calculate the diffuse attenuation coefficient (a measure of water clarity), (Acker, J., 2000).

### **3. Data**

The second leg of the cruise spent 24 hours (1 – 2 February 2002) performing continuous CTD casts across a section of the submarine canyon wall centered on 36° 48' N, 121° 49.2' W approximately six miles west of Moss Landing. The cruise took place during good weather, 1/8 cloud cover, unrestricted visibility and low sea state (<3ft). There had been several days of rain, (.24 in), the prior week providing nominal runoff into the Salinas River and the Monterey Bay during the ensuing week. This in turn increased the sediment particulate transport into the local Monterey Canyon region. Previous studies indicate a lag between river outflow sediment maximum and canyon sediment maximum reflecting short-term storage of river sediment surges on the bay shelf area (Johnson, K., 2001). These suggested that sediment would be suspended in the water column during the cruise and provide a good data set due to the previous weeks rain.

75 CTD casts were performed and data collected in series over a canyon – wall – shelf area of the upper Monterey Canyon, figure (11). The group collected an ocean observation data set with the CTD and included ship borne ADCP data at one-meter intervals during the 24-hour period. The resulting ADCP current velocity data was rotated 30° forcing a stronger u component (east west vector) representation for comparison with transmissivity and PAR data for flow up and down the canyon wall.

The data set was post processed through MATLAB and organized based on collection position of canyon, wall, or shelf. A database was created to allow use of spreadsheet and statistical charting functions in Microsoft® Excel. SURFER 7®, (Golden Software, 2000), a robust contouring and mapping tool was used to generate the horizontal and vertical cross sections for the time series. The software package used simple krigging interpolation to create a contour plotting grid field from the raw observation data set. Depth values are normalized so grid composition and interpolation schemes provide meaningful analysis between different data sets. The time is shown as year-day. Depths do not run to the actual bottom depths for the canyon – wall – shelf as a safety precaution to prevent accidental damage to the Seabird CTD. Tide data was obtained for Moss Landing using PC-Tides, and sunrise/sunset was calculated using SLAP-II in GF MPL. SeaWIFS imagery was obtained for the area from the NASA SeaWIFS project data and image archive.

#### **4. Discussion**

Figure (12) shows transmissivity (%) over the canyon position versus time. The bottom depth in the bottom of the canyon was (130-140 meters). Transmissivity in the upper 20 meters of the water column shows little variation. At year-day 33.6 a transitory event causes a slight decrease in the transmissivity values at 20 meters over the canyon that does not show up in the wall or shelf data at the same year-

day and depth. No coupling of this event to current or PAR data was observed.

The major events occur at the bottom of the water column in the canyon transmissivity data. At year-day 33.5, 33.7, and 34.05 relatively large decreases in transmissivity are noted, (10-15%). A comparison of the canyon cross section to the wall and shelf time series cross sections, figure (13) and figure (14), indicate the reduced transmissivity events at year-day 33.5 and 34.05 also occur at the bottom of the water column at both the wall and shelf positions. The decrease in transmissivity occurring at year-day 33.7 does not show up on the wall or the shelf at depth. Each of these decreased transmissivity events appears coupled to the subsurface currents at the respective positions and times.

Figure (15) shows the current structure versus time at the canyon position and correlates well visually to the transmissivity decreases at all three temporal positions. The events, at year-day 33.5 and 34.05, couple the transmissivity decrease to strong easterly currents pushing sediment up the canyon wall onto the shelf area at depth and suspending it in the water column. The event, at year-day 33.7, couples a weaker transmissivity decrease indicated only in the canyon data to a westerly current pushing sediment down the canyon wall and suspending it in the water column in the bottom of the canyon. Remember, this event is not reflected in the wall or shelf cross sections. This event is not as strong as either event associated with the easterly subsurface current. The

event at year-day 33.5 is the strongest reduced transmissivity event, (<65%) and couples to the strongest current signature. The relative magnitude of the transmissivity decrease correlates to the relative magnitude changes of the subsurface current velocity for each event.

A comparison of transmissivity horizontal cross section, figure (16) and the temperature horizontal cross section, figure (17), at 37 meters indicates the subsurface current is carrying shelf water seaward with the westerly subsurface current and upwelling canyon water unto the shelf with easterly subsurface currents. This shows up as the varying temperature structure evident in the horizontal cross section versus time. No comparison of density or salinity structure was analyzed and would be a follow on step to validate whether the water is truly canyon and shelf water undergoing property transport coupled to the subsurface current (momentum) advection. Looking at other processes, the events at year-day 33.5 and 34.05 occur concurrently with a time period 2 hours before low tide at Moss Landing, figure (18). The event at year-day 33.7 coincides with a completely different response, occurring during max flood at Moss Landing.

The next step was to investigate a link between PAR and transmissivity. The relative lack of biota in the water column this time of year would suggest no correlation. Figure (19) and figure (20) confirm the hypothesis showing the lack of correlation between the transmissivity data and the PAR data in the upper 20 meters of the water column in the

canyon and up on the shelf area. This is consistent with data analysis from (Spollen, R, 2002) where nominal correlation was shown between in-situ measurements of chlorophyll-a and SeaWIFS imagery over the area due to lower concentrations of biota in the upper water column compared to samples from other oceanic seasons. The low levels of chlorophyll-a in the water column provide a poor response for the SeaWIFs radiometer.

The lack of any correlation between transmissivity and PAR is consistent with the low biota levels in the bay and the relatively constant and consistent values of transmissivity in the upper 20 meters of the water column during the time series. It was noted many times that the water clarity appeared relatively clear visually as jellyfish were noticed in the water to 5-10 meters.

SeaWIFS imagery, figure (21), from 2 February 2002 provides additional validation to the low biota levels in the water column during the cruise. The SeaWIFS image from 2 February is consistent with February SeaWIFS climatology, figure (22). Comparison to the SeaWIFS August climatology, figure (23), shows the abundance of biologic matter in the Monterey Bay area during the late summer showing up in the SeaWIFS imagery.

The PAR data analysis, figure (24), (25), (26) over the canyon, wall, shelf area show the general tendencies expected as solar radiation begins to permeate the ocean after sunrise and continues through sunset,

(Table 1). Over the three positions; canyon, wall and shelf, the PAR data is normalized to the surface PAR value for comparison. The euphotic zone in general deepens through the day and begins to shallow as daylight wanes.

There is an anomalous feature occurring at year-day 33.8 that requires further investigation but indicates a large decrease in PAR with no related change in transmissivity in the upper 20 meters of the water column. At first it was thought it was a bad CTD but the feature was noted at all three stations with a signature in the data for 6 casts. No appreciable changes in sea state or wind are recorded in the logs and the skies remained clear throughout the entire day. A follow on comparison between PAR and fluoresce could yield an explanation.

## **5. Conclusions**

The data indicates no strong trends between transmissivity and depth over the area of observation. There are large variations in transmissivity at depth coupled to the subsurface currents. The currents may act as triggers for sediment solitons that redistribute and suspend sediment in the water column and cause sediment advection shoreward and seaward with the internal tides. No correlation was found between the transmissivity data and the PAR measurements, and the PAR values are not coupled to the subsurface or even the surface currents in the canyon. PAR values from the time series do show the correct tendencies during daylight hours. To gain a better understanding of the processes

that are taking place other data, such as density anomaly, salinity, temperature, and fluoresce data could be examined. It is critical for the Navy to continue research about the measurement and prediction of transmissivity data in support underwater optical operations and development of prediction skill.

## **7. References**

Acker, J., 2000, What is sea color. NASA, SeaWiFS Project

<http://doac.gsfc.nasa.gov/CAMPAIGN->

[DOCS/OCDST/what\\_is\\_ocean\\_color.html](http://doac.gsfc.nasa.gov/CAMPAIGN-DOCS/OCDST/what_is_ocean_color.html) , cited 14 March 2002.

Biospherical Instruments Inc.: QSP 2001 users manual, 1993. San Diego, California, 92110.

Golden Software Inc., Surfer 7 contouring and mapping package, 2000. Golden, Colorado 80401

Johnson, K.S., C.K. Paull, J.P. Barry, F.P. Chavez, 2001: A decadal record of underflow from a coastal river into the deep sea. *Geology*, **29**, 11, 1019-1022.

Pennington, J. Timothy, F.P. Chavez, 1999: Seasonal fluctuations of temperature, salinity, nitrate, chlorophyll and primary production at

station H3/M1 over 1989-1996 in Monterey Bay, California. *Deep-Sea Research II*, **47**, 947-973.

R D Instruments: Acoustic doppler current profilers, principles of operation: a practical primer, 1996. San Diego, California, 92131.

Sea Tech Inc.: Transmissometer Manual, serial number 188D, 1998. Corvallis, Oregon, 97339.

Spollen, R., 2002: Estimating primary production in central California using SeaWIFS. Naval Postgraduate School, 13 pp.

Widder, E., 1998: Ocean water: optics.

<http://www.onr.navy.mil/Focus/ocean/water/optics1.htm>. Cited 11

March 2002.

## Appendix 1: Figures

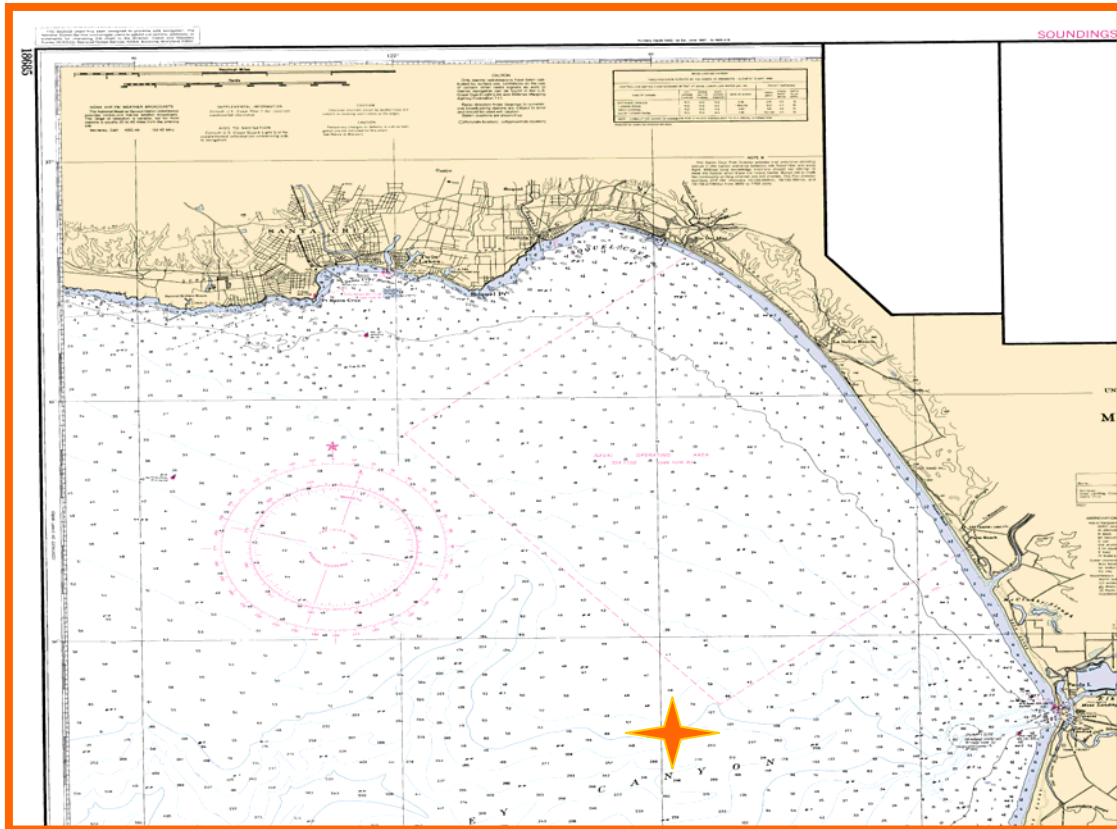


Figure 1

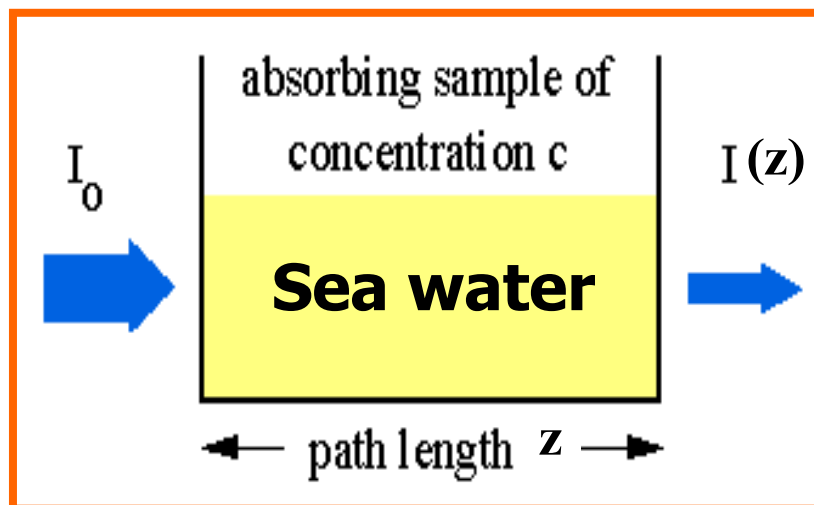


Figure 2



**Figure 3**



**Figure 4**

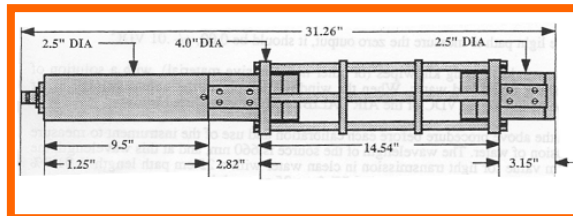


**Figure 5**

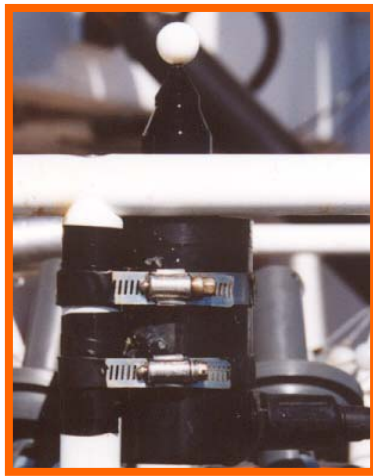


**Figure 6**



**Figure 7**

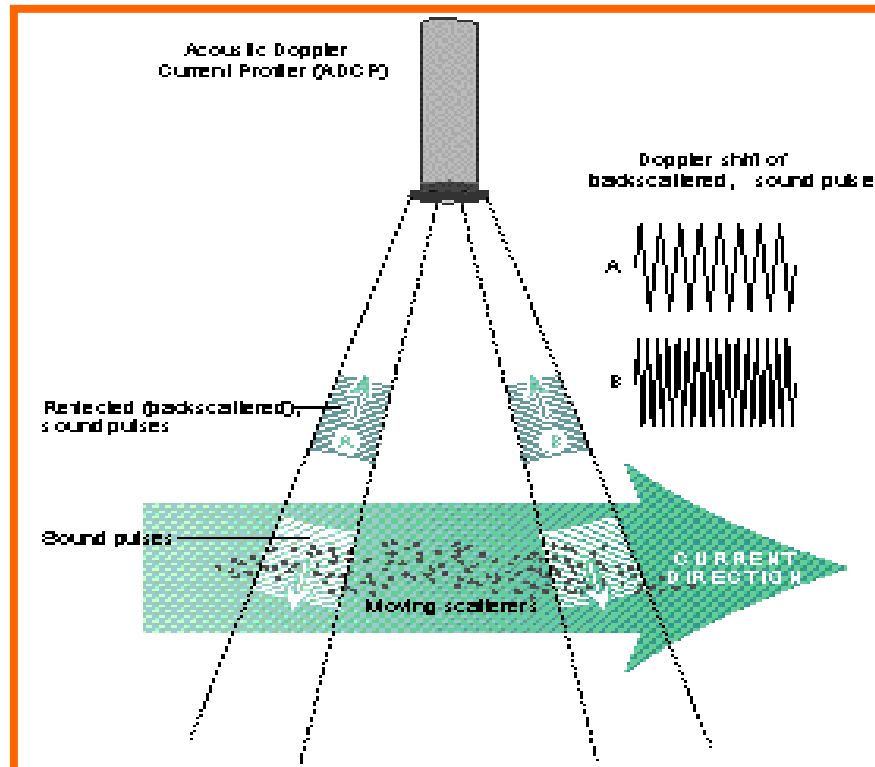


**Figure 8**

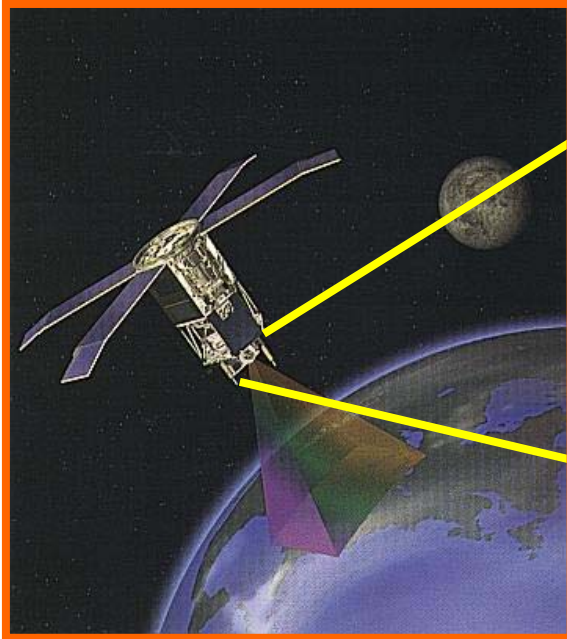


**Figure 9**

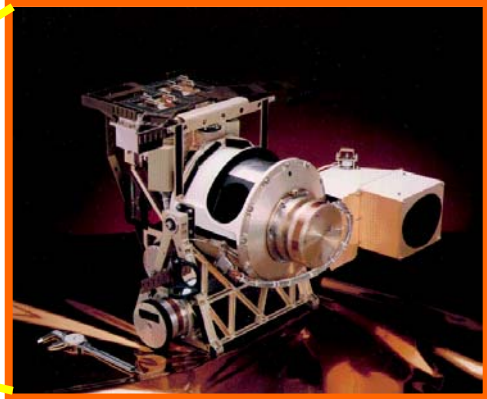


**Figure 10**

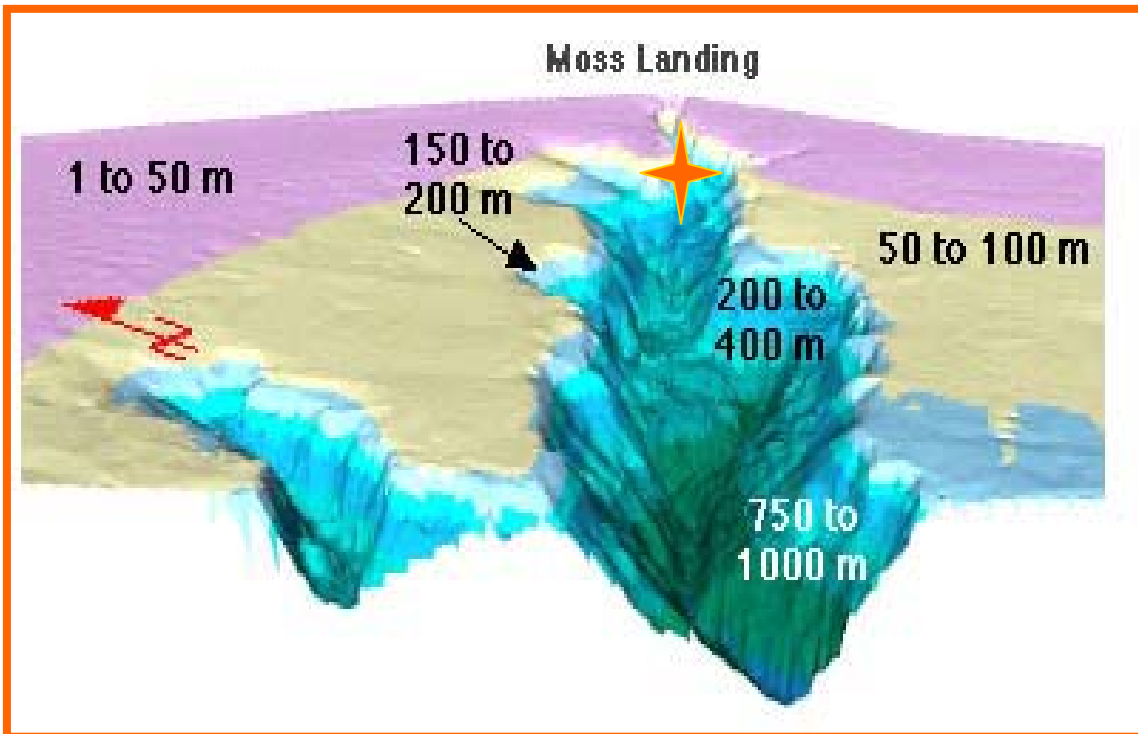


**Figure 11**

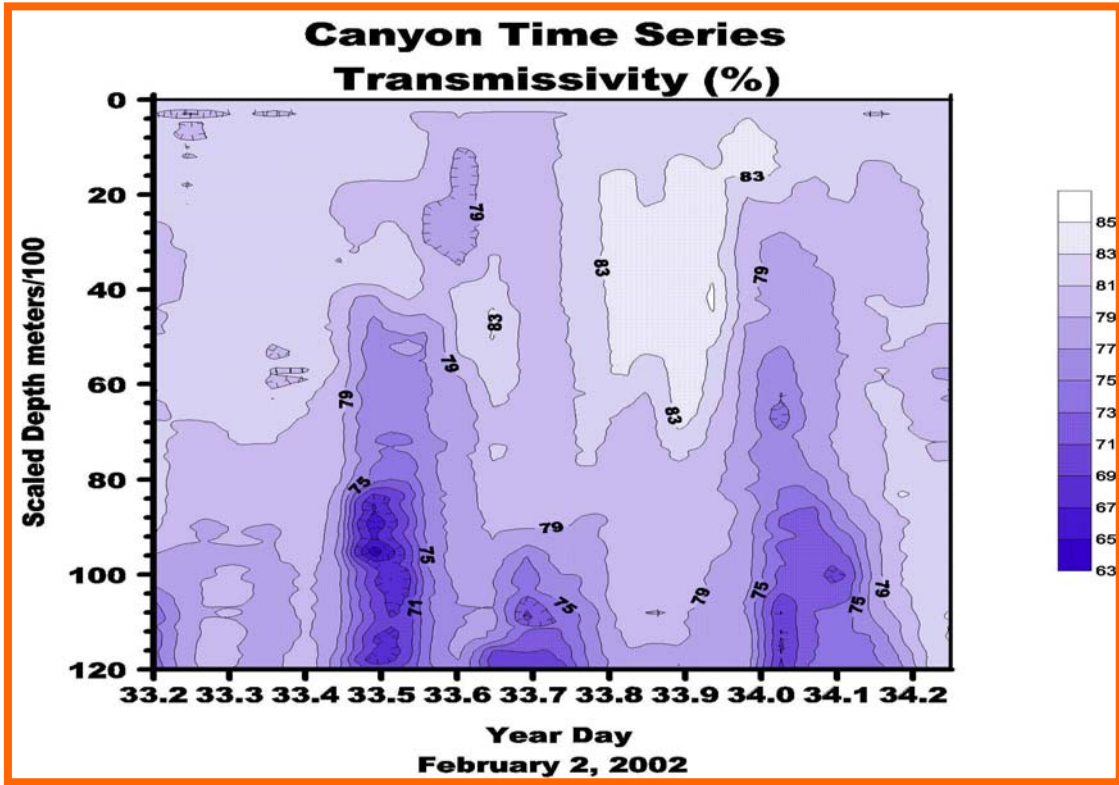


Figure 12

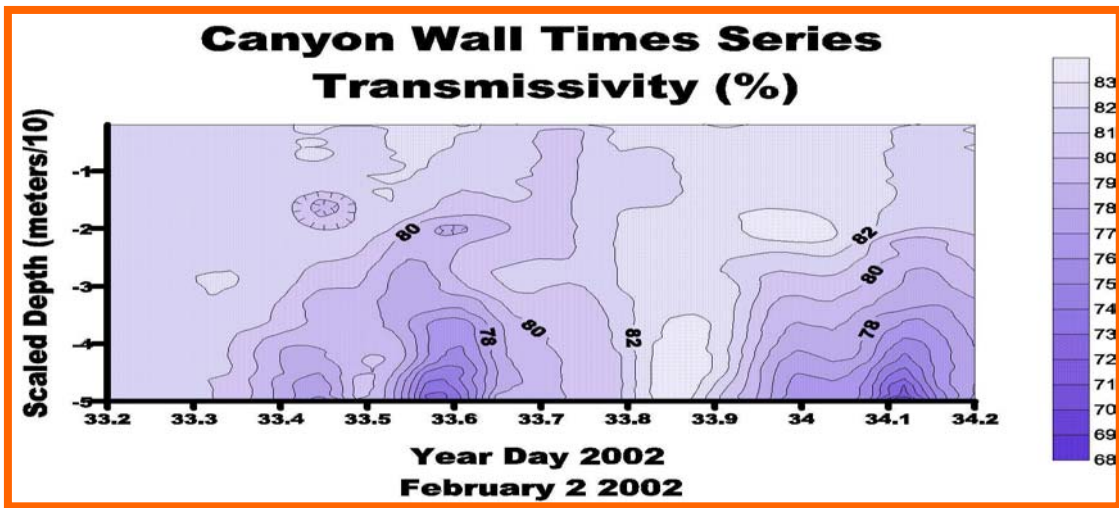


Figure 13

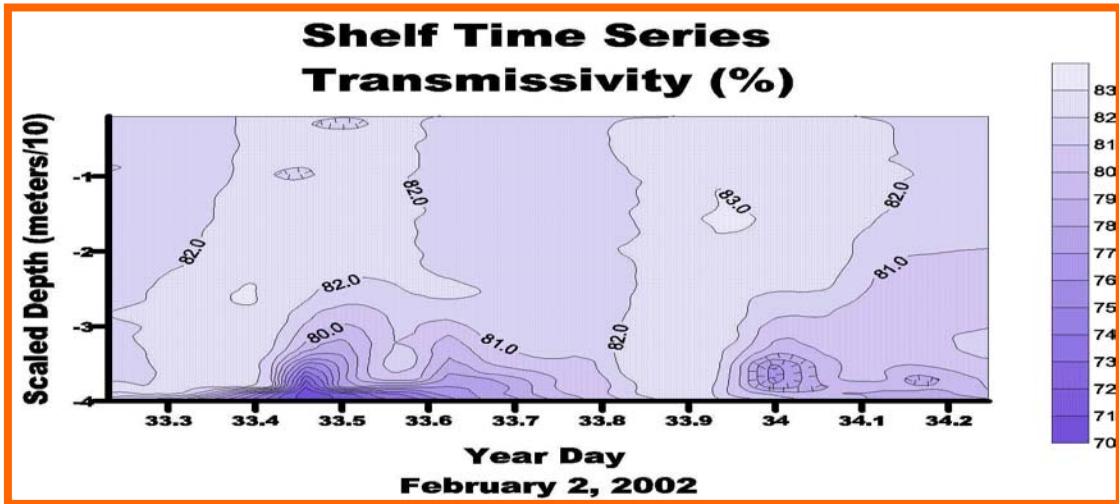


Figure 14

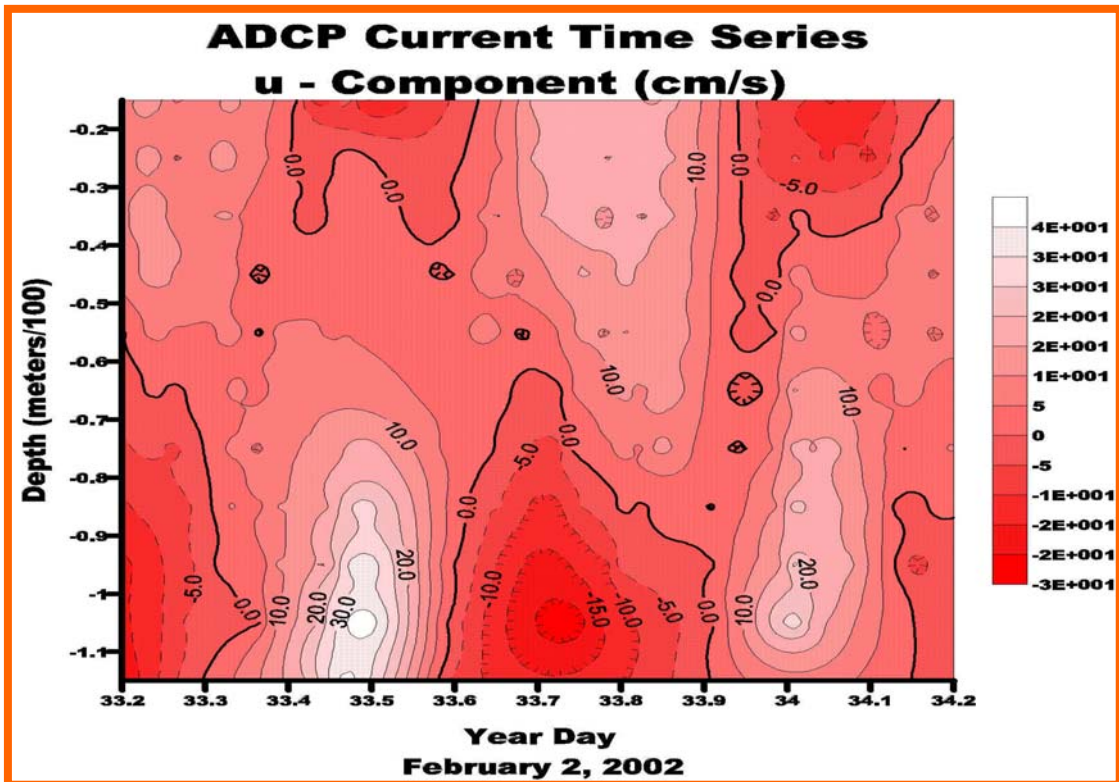


Figure 15

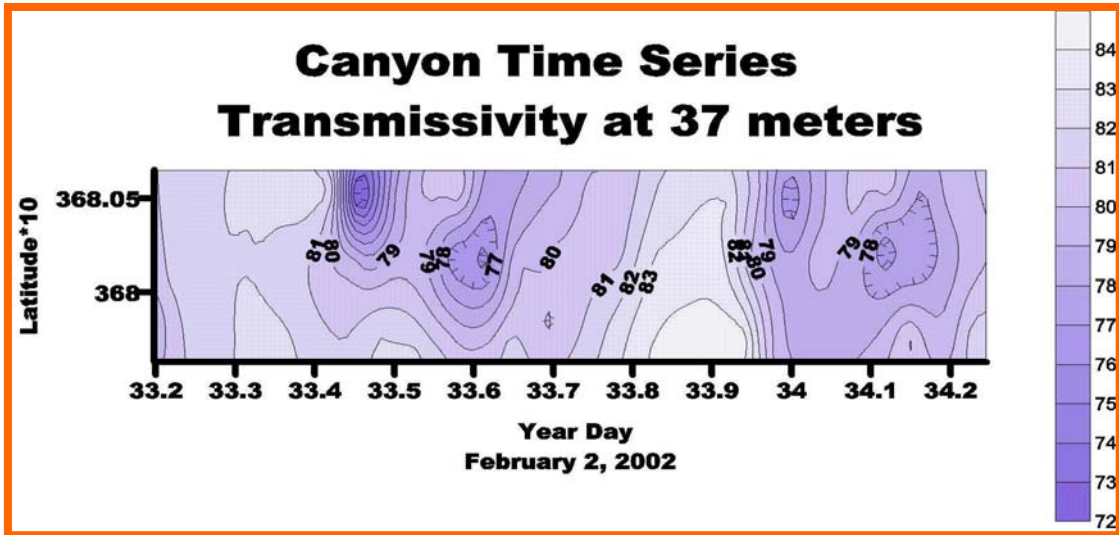


Figure 16

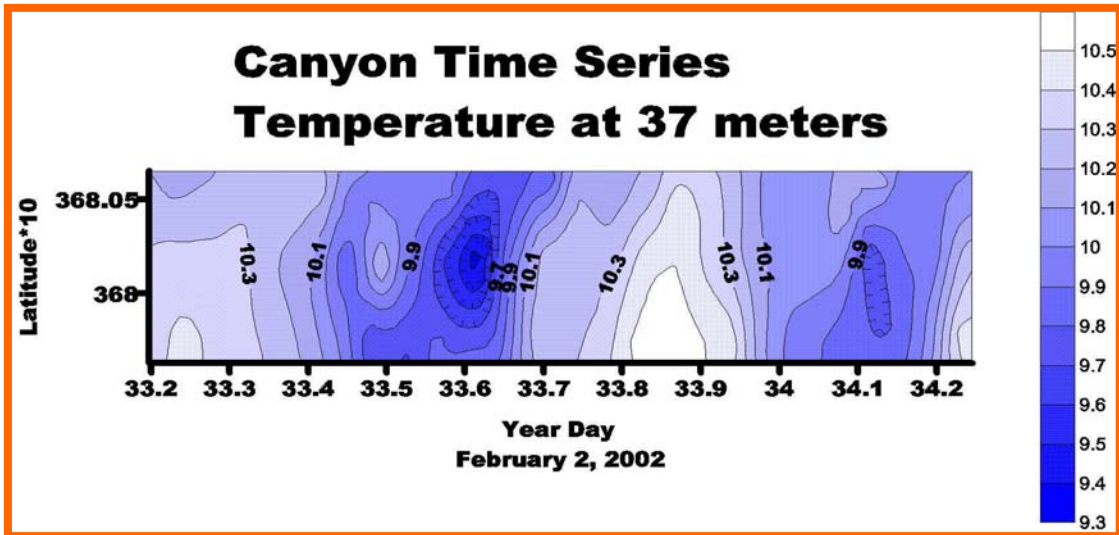


Figure 17

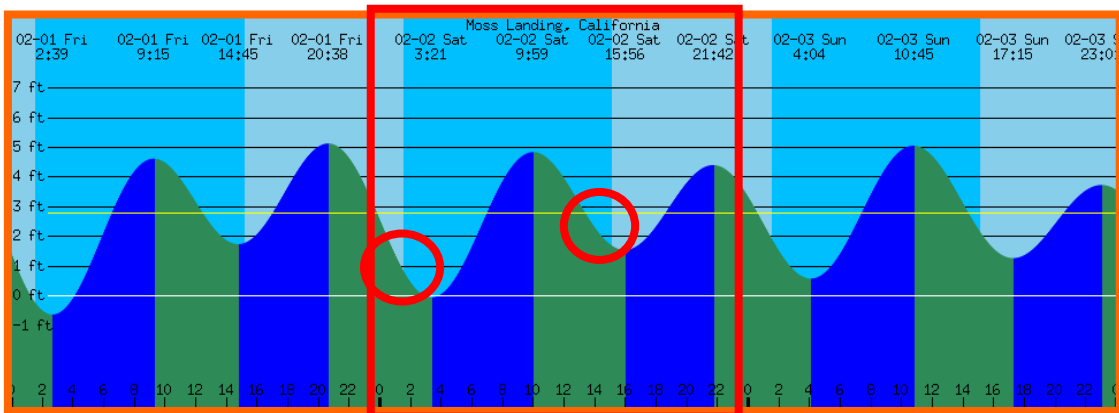


Figure 18

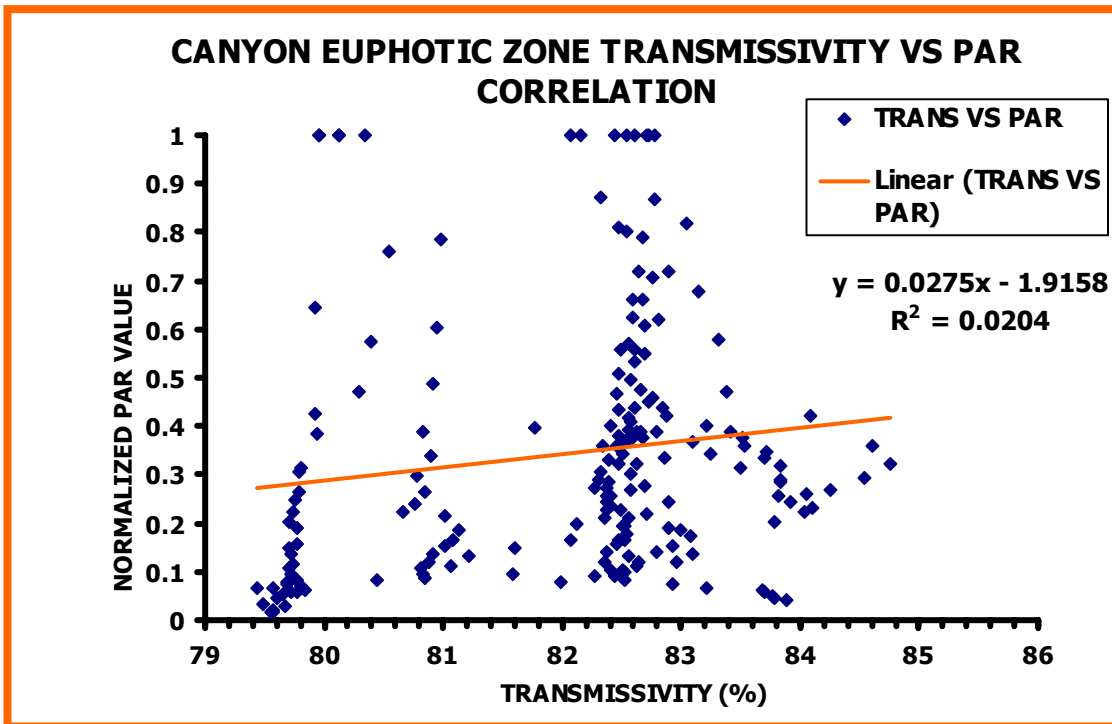


Figure 19

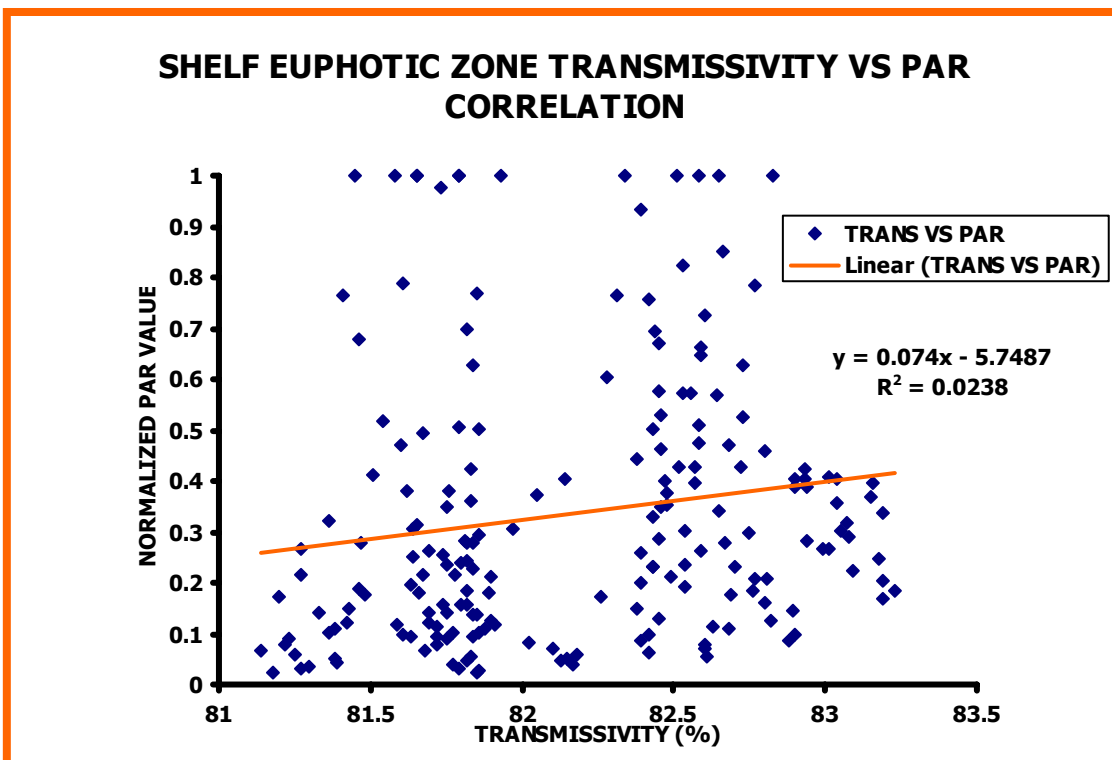
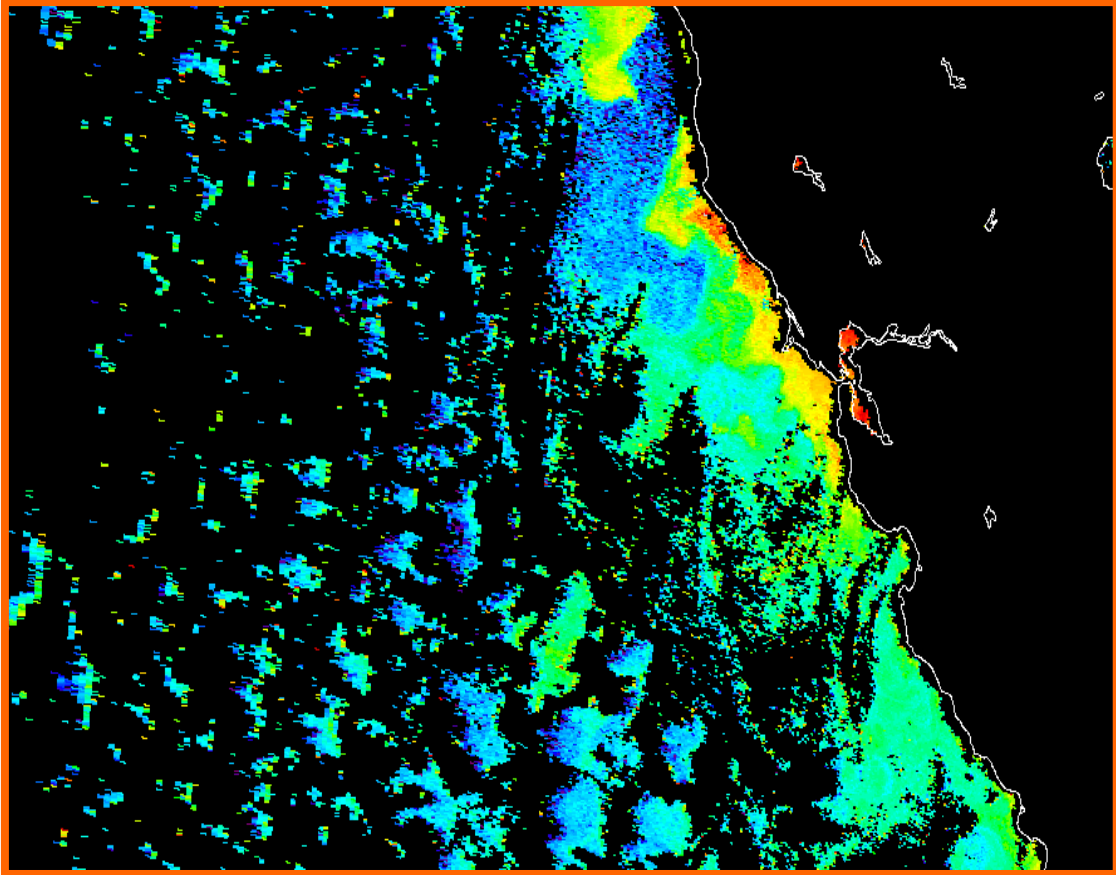
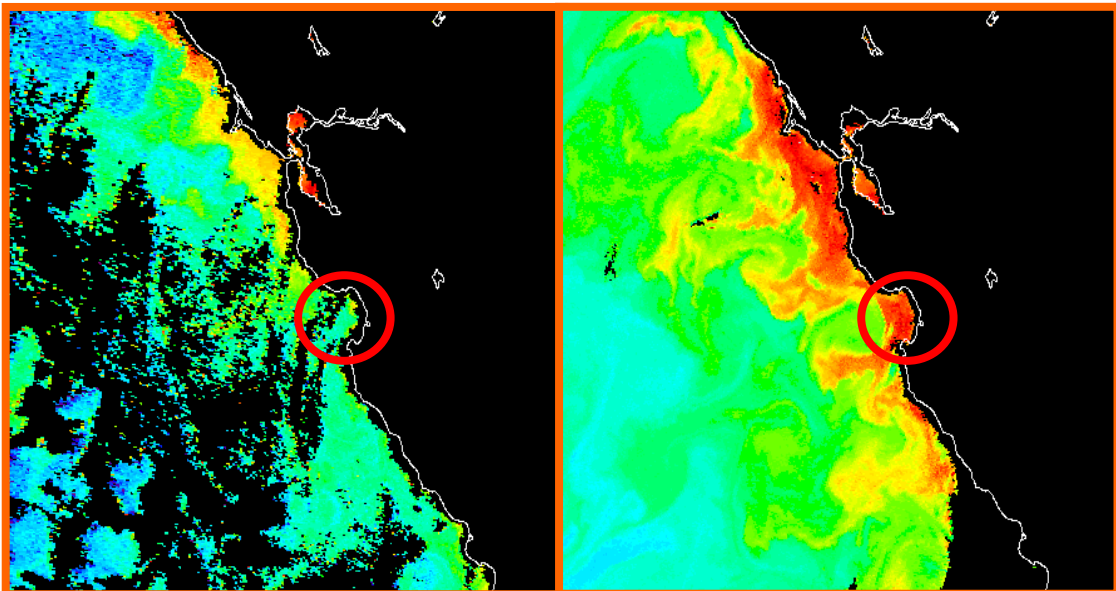


Figure 20



**Figure 21**



**Figure 22**

**Figure 23**

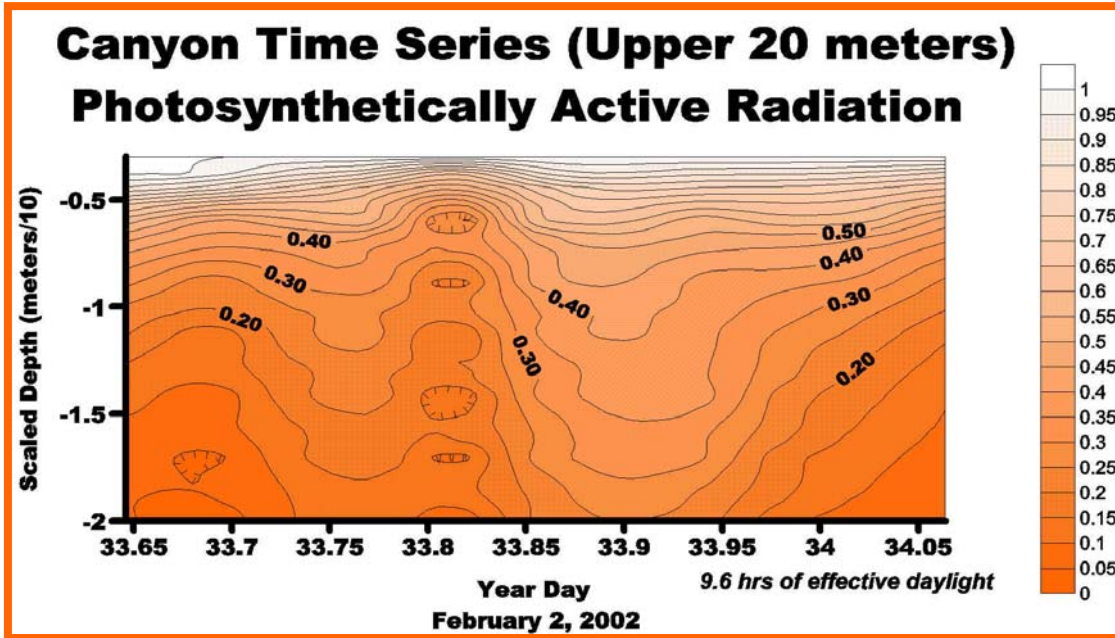


Figure 24

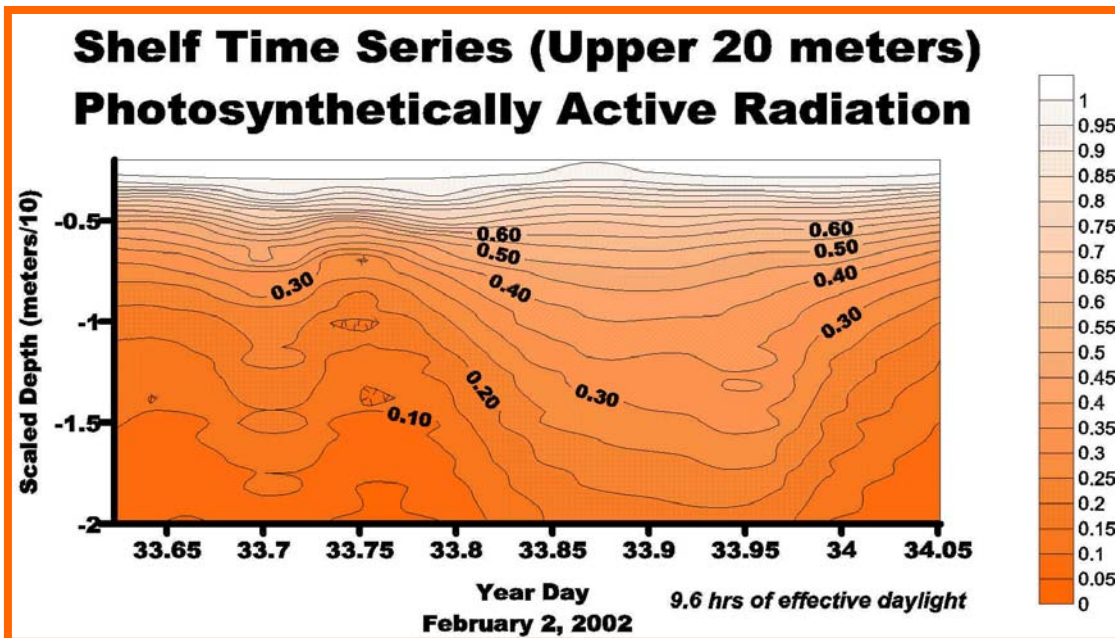
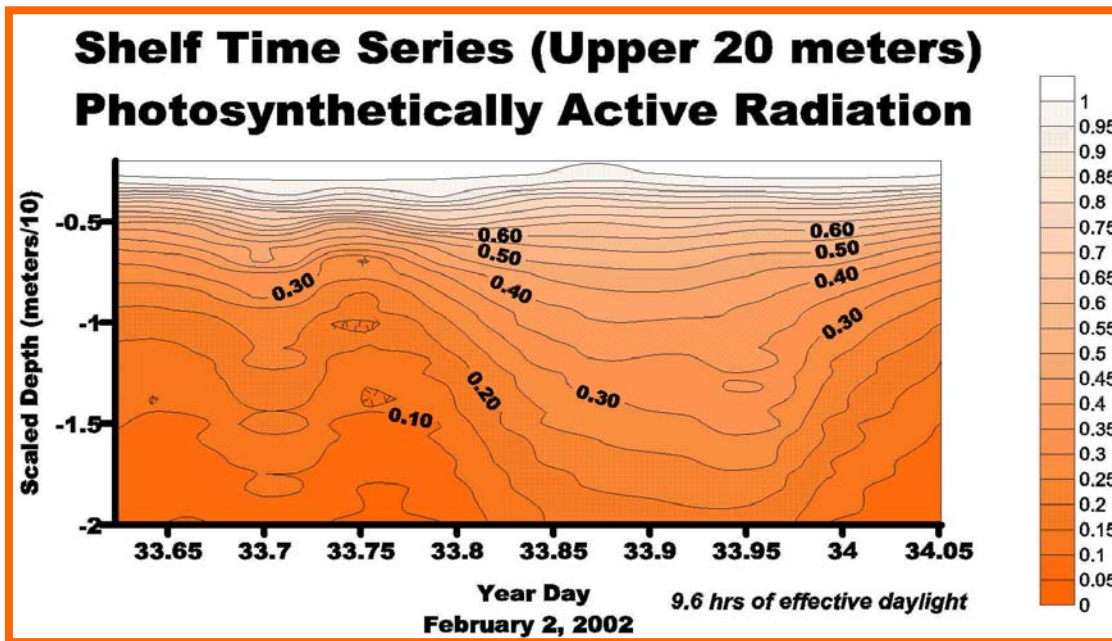


Figure 25



**Figure 26**

Saturday 2 February 2002	Pacific Standard Time
SUN	
Begin civil twilight	6:42 a.m.
Sunrise	7:09 a.m.
Sun transit	12:21 p.m.
Sunset	5:35 p.m.
End civil twilight	6:02 p.m.
MOON	
Moonrise	10:17 p.m. on preceding day
Moon transit	4:27 a.m.
Moonset	10:27 a.m.
Moonrise	11:26 p.m.
Moonset	10:59 a.m. on following day

**Table 1**